Production Mechanisms of NH and NH_2 Radicals in N_2-H_2 Plasmas

J. H. van Helden,† P. J. van den Oever, W. M. M. Kessels, M. C. M. van de Sanden, D. C. Schram, and R. Engeln*

Department of Applied Physics, Eindhoven University of Technology, P.O. Box 513, 5600 MB Eindhoven, The Netherlands

Received: April 9, 2007; In Final Form: August 12, 2007

We measured the densities of NH and NH_2 radicals by cavity ring-down spectroscopy in N_2-H_2 plasmas expanding from a remote thermal plasma source and in N_2 plasmas to which H_2 was added in the background. The NH radical was observed via transitions in the (0,0), (1,1), and (2,2) vibrational bands of the $A^3\Pi \leftarrow X^3\Sigma^-$ electronic transition and the NH_2 radical via transitions in the (0,9,0) ← (0,0,0) band of the $\tilde{A}^2A_1 \leftarrow \tilde{X}^2B_1$ electronic transition. The measurements revealed typical densities of 5×10^{18} m^{-3} for the NH radical in both plasmas and up to 7×10^{18} m^{-3} for the NH_2 radical when N_2 and H_2 are both fed through the plasma source. In N_2 plasma with H_2 injected in the background, no NH_2 was detected, indicating that the density is below our detection limit of 3×10^{16} m^{-3}. The error in the measured densities is estimated to be around 20%. From the trends of the NH_x radicals as a function of the relative H_2 flow to the total N_2 and H_2 flow at several positions in the expanding plasma beam, the key reactions for the formation of NH and NH_2 have been determined. The NH radicals are mainly produced via the reaction of N atoms emitted by the plasma source with H_2 molecules with a minor contribution from the reaction of N^+ with H_2. The NH_2 radicals are formed by reactions of NH_3 molecules, produced at the walls of the plasma reactor, and H atoms emitted by the plasma source. The NH radicals can also be produced by H abstraction of NH_2 radicals. The flux densities of the NH_x radicals with respect to the atomic radicals are appreciable in the first part of the expansion. Further downstream the NH_x radicals are dissociated, and their densities become smaller than those of the atomic radicals. It is concluded that the NH_x radicals play an important role as precursors for the N and H atoms, which are key to the surface production of N_2, H_2, and NH_3 molecules.

1. Introduction

Plasmas containing N_2 and H_2 are extensively studied because of their widespread applications in research and industry for the (surface) treatment of materials. These plasma are, for example, used for the nitriding of materials,[1] deposition of amorphous silicon nitride (a-SiN_x:H) films,[2] plasma-assisted atomic layer deposition of TaN and TiN thin films,[3,4] etching of organic low-*k* films,[5] and the chemical synthesis of ammonia.[6−9] Despite their widespread application, only limited information is available on the role of the NH_x radical species in the plasma chemistry of N_2-H_2 plasmas.

Previously, we have shown that by optimizing the atomic N and H fluxes to the surface NH_3 can be formed efficiently in plasmas generated from mixtures of H_2 and N_2; i.e., more than 10% of the total background pressure consists of NH_3.[10] The NH_3 production in N_2-H_2 plasmas is well-studied, and the NH_3 density has been predicted fairly well from a self-consistent model assuming that NH_3 is mainly produced at the surface of the plasma reactor.[1,11,12] The formation of NH_3 is generally ascribed to stepwise addition reactions between adsorbed nitrogen and hydrogen-containing radicals at the surface and incoming radicals and molecules.[12,13] NH_3 is, for example, formed by subsequent hydrogenation of adsorbed nitrogen atoms and the intermediates NH and NH_2 at the surface.

The NH and NH_2 radicals are included in models describing the plasma chemistry in N_2-H_2 plasmas. However, information on absolute densities of NH_x radicals in these plasmas is scarce. The density of NH has been determined with laser-induced fluorescence (LIF) in flowing discharges and post discharges.[14,15] The interaction of NH and NH_2 radicals with the surfaces of different materials has been addressed by Fisher and co-workers, using a NH_3 plasma molecular beam in combination with LIF for spatial imaging of the radicals.[16−18] Furthermore, mass spectrometry and emission measurements have been performed on NH_x species in the gas phase and with X-ray photoelectron spectroscopy on the surface.[13,19,20] LIF measurements on NH_2 are hampered by the effective collisional quenching of the upper electronic state (fluorescence quenching rate of 9.3×10^6 s^{-1}).[21] Moreover, absolute density measurements are difficult to carry out, because the production of a known amount of NH_2 for calibration of LIF is not a simple task. Although NH_2 has been detected with intracavity laser absorption spectroscopy[22,23] and cavity ring-down spectroscopy,[24,25] the technique was to the best of our knowledge not yet used to measure NH_2 densities in N_2-H_2 plasmas. Furthermore, to determine absolute densities of NH_x radicals spectroscopic information is needed to determine the density distribution over all possible states. Here, we present a detailed overview of the determination of absolute densities of NH and NH_2. In previous studies, we determined the density and production of NH and NH_2 radicals in $Ar-NH_3$ ($-SiH_4$) plasmas by cavity ring-down spectroscopy.[26−28]

To obtain more insight into the role of the NH_x species in N_2-H_2 plasmas, we measured the densities of NH_x ($x = 1, 2$)

* Author to whom correspondence should be addressed. Phone: +31 40 247 5786. Fax: +31 40 2456442. E-mail: r.engeln@tue.nl.

† Present address: Physical and Theoretical Chemistry Laboratory, Oxford University, South Parks Road, Oxford OX1 3QZ, United Kingdom.

10.1021/jp0727650 CCC: $37.00
Published on Web 10/12/2007

radicals at three positions in the plasma using cavity ring-down spectroscopy. Two plasmas were studied in which NH_3 generation has been observed,[9,10] both created with the expanding thermal plasma (ETP) technique. The first was an expanding N_2 plasma to which H_2 was added in the background, and the second concerned expanding N_2-H_2 plasmas with both gases applied through the plasma source. Experiments with an expanding H_2 plasma to which N_2 was added in the background will not be discussed here. In those plasmas, due to the very low ionization degree, the dissociation of N_2 molecules, necessary to form NH_x species can only be performed in a reaction with H atoms. However, this reaction is too endothermic to become effective.

The ETP technique is a remote technique in which ions and radicals are created in a high-pressure cascaded arc plasma source, and the plasma chemistry takes place downstream at a lower pressure.[29] The plasma expands supersonically through a conically shaped nozzle into a low-pressure reactor (typically 20 Pa) and, after a stationary shock, expands subsonically toward the other end of the reactor. Due to the remote nature of the technique, dissociation and ionization in the plasma source are geometrically separated from the plasma chemistry in the reactor. In this way, plasma production, plasma transport, and plasma−surface interactions are separated, meaning that the plasma conditions can be controlled independently from the downstream plasma chemistry. This allows independent studies of the different aspects of the process in a relatively simple manner.

In this work, the plasma source is fed with N_2 (with H_2 added in the background) or with mixtures of N_2 and H_2. When operating the arc on pure N_2, the N/N_2 ratio at the plasma source exit is estimated to be 0.5, corresponding to a dissociation degree of 35% and a N flow of 6 sccs (standard cubic centimeters per second) using a total N_2 flow of 17 sccs. An ionization degree at the exit of the arc of around 1% is attained, which means a N^+ flow of less than 0.3 sccs.[30,31] Pure H_2 source operation yields dissociation degrees on the order of 10%, thus at maximum an H flow of 3 sccs.[31] We will assume the H and N flows from a N_2-H_2 arc source to be similar to the pure N_2 or H_2 operation. We are now interested in the NH and NH_2 densities and their formation kinetics in these plasmas.

After describing the basics of the ETP technique (section 2.1), we will discuss in section 2.2 the experimental details of the cavity ring-down setup used to measure the NH and NH_2 radicals. In the results section (section 3), the measured spectra and densities of the NH_x radicals will be presented, and in section 4 the main reactions in the plasma leading to the observed NH_x radical densities will be discussed. In the last section, the conclusions are presented.

2. Experimental Details

2.1. Expanding Thermal Plasma Setup. The plasmas from mixtures of N_2 and H_2 were created with the ETP technique. The technique has been described extensively in the literature (see, e.g., refs 29 and 33). Here, only a short description of the main constituents of the setup is given. In the direct current (DC) cascaded arc plasma source a subatmospheric (typically 20 kPa) plasma is created with a power of around 5 kW. The cascaded arc source consists of a 4 mm diameter narrow and 30 mm long channel created by five stacked water-cooled insulated copper plates. The cascaded plates are at floating potential. The last plate acts as the common anode for the discharge. A gas flow is admitted to the channel, and a DC current is drawn from the three cathodes to the grounded anode plate producing the plasma. Due to the high pressure and high power density, the plasma is close to local thermal equilibrium ($T_{\text{heavy particles}} \simeq T_e$) and characterized by a high electron density $n_e \approx 10^{22}$ m^{-3} and a modest electron temperature $T_e \approx 1$ eV. The heavy particle temperature of approximately 1 eV leads to almost full dissociation of molecular gases when these are injected in the arc. The pressure gradient between the source (>100 kPa) and the reactor (typically 20 Pa) causes the plasma to expand supersonically into the reactor. (The expansion axis is denoted as the *z*-axis.) At approximately 3.5 cm from the exit of the source, i.e., the so-called nozzle, a stationary shock is formed (see section 2.2). Behind the shock the plasma flows subsonically toward the other end of the reactor. As there is no power dissipation anymore in the reactor, the plasma is recombining. In the expansion, the electron temperature T_e decreases to 0.1−0.3 eV, and the electron density downstream is on the order of 10^{18} m^{-3}. The electron temperature is too low for electron-induced dissociation or excitation processes to play a role.[29] The primary reactive particles in the expansion are the ions or atomic radicals.

Molecular gases can be injected into the background of the plasma reactor, i.e., into the recirculation flow in the reactor.[34] The injected molecules, together with molecules generated by the plasma itself (possibly in interaction with a surface), form the basis of influx into the expanding plasma beam. It has been established that diffusion inward occurs mainly in the subsonic region. However, if the flow is rarefied, then the background gas can invade the plasma expansion already in the supersonic region.[35,36] As a result, the gas mixture in the recirculation flow in the periphery of the reactor is mixed into the plasma emanating from the source. The molecules diffusing into the expanding plasma can undergo charge transfer and subsequently dissociative recombination reactions with mainly the N^+ ions emanating from the source, leading to atomic and/or molecular radicals. Furthermore, the molecules diffusing into the beam may undergo abstraction reactions with atomic radicals, leading to additional radicals. Direct generation of molecules in the volume by three-particle reactions from atomic or molecular radicals can be excluded, because these reactions are too slow to lead to any significant production under our low-pressure conditions (mostly <100 Pa). Furthermore, the transit time from the plasma source to the other end of the plasma reactor, relevant for "forward'' kinetics, is short (<1 ms), so two-particle reactions in the plasma beam can be neglected. However, the residence time, relevant for background kinetics, is relatively long (0.1−1 s), so there two-particle reactions can take place.

We studied two different experimental situations: expanding N_2 plasmas with H_2 injected in the background and expanding N_2-H_2 plasmas as schematically depicted in Figure 1. In both plasmas, the generation of NH_3 in the downstream section is observed.[9,10] The formation of NH_3 molecules in the background by bimolecular N_2-H_2 gas-phase reactions involving atomic and molecular radicals can be excluded, because processes leading to NH_3 at typical temperatures for the radicals in the background of 1000 K are too slow to lead to production. The formation of molecules at the surface is much more likely; the surface acts as the third body in this case. This means that most of the (atomic) radicals will arrive at the surface at which they will adsorb or reflect. If reflected, then the density close to the surface will increase until the consumption by adsorption is equal to the production of that radical. At the surface, new molecules can be generated that subsequently desorb. This process is called plasma-activated catalysis, because a plasma is used to produce the radicals for the molecule production at

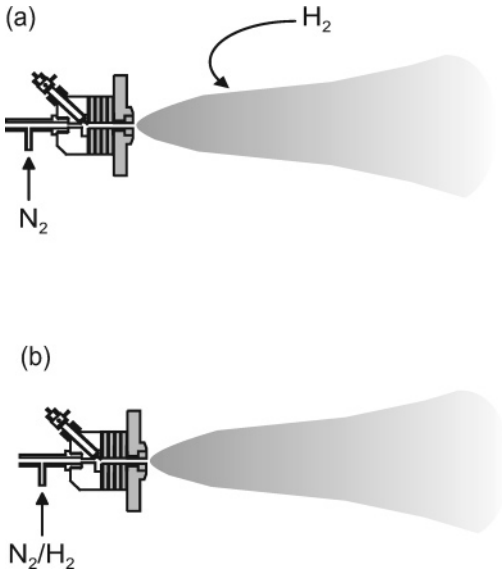

Figure 1. Schematic representation of the expanding plasma jet for both types of plasmas: (a) expanding N_2 plasma to which H_2 was injected in the background; (b) expanding N_2-H_2 plasma.

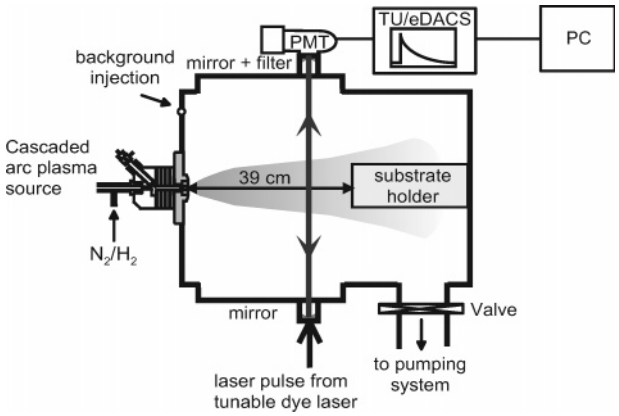

Figure 2. Schematic representation of the expanding thermal plasma (ETP) setup together with the cavity ring-down setup including a TU/eDACS data acquisition system.

the surface.[9] Note that the produced molecules may still undergo reactions in the recirculation flow in the background of the plasma reactor during the lifetime of (active) particles in the background.

To measure absolute concentrations of the stable gas species N_2, H_2, and NH_3, the setup was equipped with a residual gas analyzer to perform mass spectrometry measurements. The gas analyzer was situated on top of the reactor at 56 cm from the source and was calibrated by injecting the relevant gases into the plasma reactor at various known pressures in the absence of a plasma.

2.2. Cavity Ring-Down Spectroscopy. *2.2.1. Principle.* We measured the density of NH and NH_2 radicals in the downstream plasma using cavity ring-down spectroscopy (CRDS) at three positions on the axis ($z = 10$, 21, and 36 cm) from the plasma source (Figure 2). CRDS is an absolute absorption technique based on the measurement of the decay rate of a light pulse confined in an optical cavity rather than the magnitude of the absorption.[37] The optical cavity is formed by two high-reflectivity plano-concave mirrors. The effective multipassing of the laser pulse within the optical cavity makes CRDS a highly sensitive technique. Furthermore, the technique is insensitive to light intensity fluctuations of the light source and is therefore not affected by pulse-to-pulse fluctuations of the laser system. The exponential decay of the light leaking out of the cavity can be expressed by a ring-down time τ. When an optical cavity contains no absorbing medium, the decay is solely caused by transmission and scattering losses and is given by $\tau_0(\nu) = d/(c|\ln R(\nu)|)$. Herein d is the length of the cavity, c is the speed of light, and $R(\nu)$ is the reflectivity of the mirrors. For a cavity consisting of high-reflectivity mirrors ($R \approx 1$), this can be rewritten as $\tau_0(\nu) = d/(c(1 - R(\nu))$. When an absorbing medium is present in the cavity, the decay becomes faster and is expressed by means of a ring-down time $\tau(\nu)$

$$\tau(\nu) = \frac{d/c}{1 - R(\nu) + A(\nu)} \quad (1)$$

The frequency-dependent absorption per pass $A(\nu)$ can be rewritten as $A(\nu) = n_{v,J}\sigma(\nu)l$, where $\sigma(\nu)$ is the frequency-dependent cross-section, l is the absorption path length, and $n_{v,J}$ is the number density in the lower level of the transition of the absorbing species. When the absorption cross-section is known, the absorption per pass $A(\nu)$ can easily be obtained by measuring the ring-down time with and without absorbing medium.

2.2.2. Absorption Path Length. The cavity ring-down measurements were performed in the subsonic region of the expansion. Previously reported results on plasma expansions show that the plasma beam diameter at the position, Z_M, of the stationary shock is roughly 2 times Z_M.[35] Z_M can be calculated[38] and is around 3.5 cm. Diffusion of particles out of the plasma beam has previously been observed for N and H atoms in N_2 and H_2 plasmas. The diffusion is induced by the density gradient for these radicals between the plasma beam and the periphery caused by surface association.[30,39] In our calculation of the density of the radicals, we used an absorption path length in the plasma of 0.1 m at $z = 10$ cm, taking into account that with increasing distance from the plasma source the absorption path length increases due to the diffusion of NH and NH_2 radicals out of the plasma beam. The absorption path lengths at $z = 21$ and 36 cm are estimated to be, respectively, 0.2 and 0.3 m. This is based on the comparison of cavity ring-down measurements with threshold ionization mass spectrometry and model calculations of the radial distribution of radicals in the plasma beam using the commercial computational software Phoenics-CVD taking into account basic gas-phase and surface chemical processes in the plasma.[40,41] In the density calculations, a uniform density distribution of the radicals over the absorption path length is assumed. The overall experimental accuracy of the obtained densities is about 20%.

Reactions between radicals and ions in the plasma beam and N_2 and H_2 molecules diffusing into the plasma beam first occur at the outside of the plasma beam.[34,42,43] This effect would result in a smaller effective absorption path length and thus an overestimation of the radical density by a factor of 2 in this paper.

2.2.3. Optical System. A tunable Sirah PrecisionScan-D dye laser pumped by the second harmonic output of a Nd:YAG laser (Spectra-Physics GCR-4) produced ~8 ns laser pulses at a repetition rate of 10 Hz. To measure NH absorptions, the dye laser was operated on pyridine 1 dye to create laser light around 680 nm. The laser beam was subsequently frequency-doubled using a potassium dihydrogen phosphate (KDP) crystal, resulting in laser pulses around 340 nm. To measure NH_2 absorptions, the dye laser was operated on rhodamine B, resulting in laser light around 600 nm. To avoid optical saturation of the transitions of interest, a UV attenuator was placed in the laser beam in the first experimental configuration, and in the latter experiment the amplifier stage of the dye laser was not

implemented. The intensity of the laser pulses was further reduced by a set of filters, leading to a typical pulse energy of ~100 μJ in front of the cavity.

The laser pulses were coupled into a 1.12 m long optical cavity formed by two high-reflectivity plano-concave mirrors. The mirrors were mounted on flexible bellows for accurate alignment, which were directly flanged onto the stainless steel reactor in which the plasma expanded. The mirrors (Laser-Optik) had a diameter of 1 in., a radius of curvature of $r = -1$ m, and a reflectivity of $R \approx 0.997$ at 340 nm for the NH detection and a reflectivity of $R \approx 0.999$ at 560 nm for the NH_2 detection. Immediately in front of the mirrors an argon flow was injected to protect the mirrors from reactive plasma species. The light leaking out of the cavity through the second mirror was detected by a photomultiplier tube (Hamamatsu R928) placed closely behind the cavity to ensure that all cavity modes were detected with equal probability. An interference band-pass filter in front of the photomultiplier shielded the detection system from the plasma light.

The CRD transient of every laser shot was individually processed by means of a state-of-the-art 100 MHz, 12 bits data acquisition system (TU/eDACS[44,45]). All recorded CRD transients were single-exponential and were analyzed by a weighted least-squares fit of the logarithm of the transient, yielding the ring-down time of the light intensity in the cavity. To improve the signal-to-noise ratio, the averaged ring-down time of 20 laser shots was taken for all measurements. The baseline of the NH_2 spectra was affected by an oscillating behavior of the CRD signals and is caused by interferometric fringes with a free spectral range consistent with the mirrors' thickness. This behavior hampered the baseline correction procedure and resulted in a slightly lower experimental accuracy compared to the NH measurements. The integrated absorption as a function of the laser energy coupled into the cavity was measured to be constant for both NH and NH_2 radicals. This shows that optical saturation was avoided at all laser energies used during the experiments.

3. Results

3.1. Determining Absolute Densities of the NH_2 Radical. The NH_2 radical was observed via transitions in the (0,9,0) ← (0,0,0) band of the $\tilde{A}^2A_1 \leftarrow \tilde{X}^2B_1$ electronic transition around 597.5 nm. The radical is a highly asymmetric top molecule with an angle around 110° in the ground state, while it has a nearly linear configuration in the excited state. The electronic band spectrum ($\tilde{A}^2A_1 \leftarrow \tilde{X}^2B_1$) of NH_2 in the visible (380−830 nm) consists mainly of transitions of a long progression of bands $(0,\nu_2,0) \leftarrow (0,0,0)$ of the bending vibration of NH_2.[46] (The notation for ν_2 used in this section is according to the linear molecule convention. The correlation between the linear and bent notation for vibrational numbering is: $\nu_2(\text{linear}) = 2\nu_2(\text{bent}) + K_a + 1$.) Figure 3 shows a typical spectrum containing lines of the $^PQ_{1,N}$ branch of the Σ vibronic sub-band as measured in a N_2-H_2 plasma at a position of $z = 21$ cm from the plasma source. The rotational branch is denoted as $^{\Delta K_a}\Delta N_{K_a,K_c}$,[46] where K_a and K_c are the quantum numbers of rotation about the *a*- and *c*-axes. The line positions and rotational assignments are obtained from Ross et al.[47] The transitions in this branch obey the *c*-type selection rules: $\Delta J = \Delta N = 0$, $\Delta K_a = -1$, and $\Delta K_c = 0$. Furthermore, each line with quantum number *N*, the total angular momentum apart from electronic spin, consist of two levels F_1 and F_2 due to spin-rotation splitting. The F_1 levels have $J = N + 1/2$, and the F_2 levels have $J = N - 1/2$. The lines marked by a cross in Figure 3 are not part of the $^PQ_{1,N}$ branch

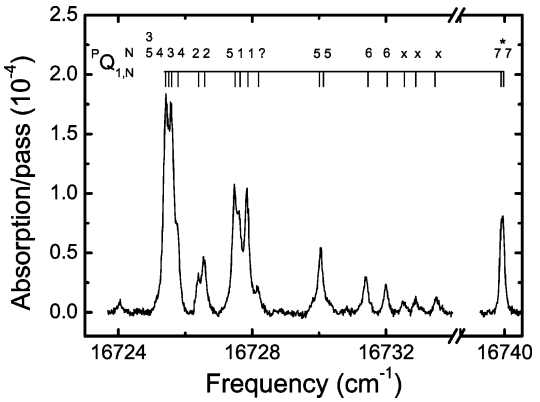

Figure 3. Part of the NH_2 spectrum as measured with cavity ring-down spectroscopy at $z = 21$ cm. The plasma source was operated on a mixture of 5 sccs N_2 and 11.67 sccs H_2 at an arc current of 55 A. The background pressure was 20 Pa. The line positions reported in the literature are indicated by ticks in the upper part of the graph, and the rotational assignments for the $^PQ_{1,N}$ branch of the Σ vibronic sub-band are given.[47] The "isolated'' spin doublet $^PQ_{1,N}(7)$ line at 16 739.90 cm^{-1} was used for the density measurements (marked by an asterisk). The lines marked by a cross are lines that are not part of the $^PQ_{1,N}$ branch. The line marked with a question mark has not been assigned.

of the Σ vibronic sub-band but are assigned in the literature as a line of the $^RR_{1,N}$ branch of the Δ vibronic sub-band (left cross) and lines of the $^PP_{1,N-1}$ branch of the Σ vibronic sub-band. The line marked with a question mark is not assigned in the literature. The spin doublet line $^PQ_{1,N}(5)$ at a center frequency of 16 730.07 cm^{-1} is associated with a multiple perturbation.

The density of NH_2 was determined by scanning the laser over the "isolated'' spin doublet line $^PQ_{1,N}(7)$ at a center frequency of 16 739.90 cm^{-1} (597.375 nm) (marked by an asterisk in Figure 3). This line is the most studied NH_2 transition because it is an isolated line and is therefore one of the few lines of the NH_2 absorption spectrum for which the oscillator strength has been reported.[48,49] To determine the integrated absorption of the spin doublet line and its line profile, the doublet splitting was set to a value of 3.44 GHz, and the ratio of the area of the two components of the doublet line was set at 0.82, as determined by Friedrichs et al.[24] The density of NH_2 in the lower state of the $^PQ_{1,N}(7)$ transition was obtained using a value of the integrated absorption cross-section of $\sigma_{\text{int}} = 7.4 \times 10^{-21}$ m^2 cm^{-1}, which was calculated from the oscillator strength reported in the literature by Votsmeier et al.[49] (see ref 26). The density calculated in this way is insensitive to the laser line width and the Doppler broadening effect.

The total NH_2 density was calculated by taking into account the density distribution over all possible states, which is determined by the kinetic, rotational, and vibrational temperatures of the NH_2 radicals. The kinetic gas temperature of the radicals was obtained from the Doppler broadening by deconvoluting the experimental absorption lines into a Lorentzian laser profile and a Gaussian Doppler contribution. This procedure yielded a Lorentzian laser line width of 0.064 ± 0.01 cm^{-1} at 16 739.90 cm^{-1}, which is consistent with the manufacturer's specifications[50] and previous values determined for this laser system.[44] From all of the measured $^PQ_{1,N}(7)$ lines and the spectra, an average NH_2 kinetic gas temperature of 1775 ± 200 K was determined at $z = 10$ and 21 cm from the plasma source and 1350 ± 250 K at $z = 36$ cm. The measured temperatures point to the fact that these NH_2 radicals are only present in the plasma beam and not in the periphery, where the temperatures are much lower. The NH_2 kinetic gas temperature is in agreement with previous measured temperatures of NH_x radicals in expanding

$Ar-NH_3$ plasmas,[26] with measured temperatures of radicals in expanding plasmas of different gas mixtures,[44] and with the temperature of H atoms in, for example, $Ar-H_2$ plasmas as measured with two-photon absorption laser-induced fluorescence (TALIF).[51] These measurements all concerned radical species, which are primarily present in the plasma beam and not (or much less) in the periphery. The rotational and vibrational temperatures of the NH_2 radicals could not be determined. It can be argued that because the NH_2 kinetic gas temperature reflects the gas temperature in the plasma expansion the NH_2 radicals in the plasma are already thermalized by elastic collisions with other particles. To validate this, spectra over a broader wavelength range than was possible with the setup have to be measured. We therefore assume that the rotational and vibrational temperatures are equal to the kinetic gas temperature. If a non-Boltzmann distribution of the NH_2 radicals is assumed, then the densities would change by not more than a factor of 2 (assuming a similar distribution as for NH).

We calculated the total NH_2 density assuming a Boltzmann density distribution over the rotational and vibrational energy states with a rotational and vibrational temperature of 1775 K for $z = 10$ and 21 cm and 1350 K for $z = 36$ cm. The Boltzmann fraction f_B for NH_2 is reported in the literature by Green and Miller[52] and Kohse-Höinghaus et al.[48]

$$f_B = \frac{3}{4}\frac{(2J''+1)}{g''Q_rQ_v}\exp\left[-\frac{E_{rot}}{kT_{rot}}\right]\exp\left[-\frac{E_{vib}}{kT_{vib}}\right] \qquad (2)$$

The factor of $^3/_4$ occurs due to the nuclear spin of the H atoms, J'' and g'' are the total rotational quantum numbers including spin and the electron-spin degeneracy of the lower state, Q_r and Q_v are the rotational and vibrational partition functions, E_{rot} and E_{vib} are the rotational and vibrational energies of the lower state, and T_{rot} and T_{vib} are the rotational and vibrational temperatures, respectively. We note that g'' is equal to 1, because the integrated absorption of the measured line contained both components of the spin doublet. The partition functions Q_r and Q_v are given by Green and Miller.[52] E_{vib} is given by Herzberg,[53] and $E_{rot} = hcF(J)$, in which $F(J)$ is the experimentally determined rotational term value as reported by Ross et al.[47] The total NH_2 density (m^{-3}) at $z = 10$ cm can then be calculated from the integrated absorption A_{int} (cm^{-1}) using an absorption path length $l = 0.1$ m and $T = 1775$ K

$$n_{NH_2} = \frac{A_{int}}{\sigma_{int}l}\frac{1}{f_B} = (2.3 \pm 0.5) \times 10^{23}A_{int} \qquad (3)$$

The complete derivation of the total density of NH_2 is given in ref 26.

The oscillator strengths of the other transitions in the $^PQ_{1,N}$ branch are not known. In Table 1, the oscillator strengths of the measured transitions in the $^PQ_{1,N}$ branch are presented as determined from the spectrum depicted in Figure 3 assuming a Boltzmann density distribution at 1775 K. We also determined the oscillator strengths for the same transitions from the spectrum published in Figure 4 of Rahinov et al.,[25] in which NH_2 was measured under conditions in which a Boltzmann density distribution can be assumed. They measured a NH_2 spectrum produced by NH_3 pyrolysis in a quartz cell at 890 K and at a pressure of 1.6 kPa. The obtained oscillator strengths using a Boltzmann distribution at 890 K are also presented in Table 1. Despite the fact that the oscillator strengths were determined in the same manner for both spectra and using the absorption path length as given by Rahinov et al., our oscillator strengths are higher at lower N up to a factor 3.5. This could be caused by the fact that the spectrum obtained by Rahinov et al. was measured at a lower temperature and is thus less affected by Doppler broadening in comparison with our spectra. As a result of Doppler broadening, especially the lower J transitions in our spectrum are overlapping more strongly, which hampered the determination of the integrated absorption of the absorption line.

TABLE 1: Oscillator Strengths for Part of the Transitions in the $^PQ_{1,N}$ Branch of the Σ Vibronic Sub-band in the (0,9,0) ← (0,0,0) Band of the $\tilde{A}^2A_1 \leftarrow \tilde{X}^2B_1$ Electronic Transition of NH_2[a]

rotational assignment	frequency (cm^{-1})	oscillator strength (this work)	oscillator strength (ref 25)
$^1{1_{01}}-{}^1{1_{11}}$	16 727.872	3.52×10^{-4}	1.05×10^{-4}
$^2{1_{01}}-{}^2{1_{11}}$	16 727.638	4.76×10^{-4}	1.63×10^{-4}
$^1{2_{02}}-{}^1{2_{12}}$	16 726.579	1.02×10^{-4}	4.47×10^{-5}
$^2{2_{02}}-{}^2{2_{12}}$	16 726.398	8.20×10^{-5}	4.15×10^{-5}
$^1{3_{03}}-{}^1{3_{13}}$	16 725.594	2.93×10^{-4}	1.04×10^{-4}
$^1{4_{04}}-{}^1{4_{14}}$	16 725.784	9.27×10^{-5}	3.75×10^{-5}
$^2{5_{05}}-{}^2{5_{15}}$	16 727.488	1.52×10^{-4}	7.63×10^{-5}
$^1{6_{06}}-{}^1{6_{16}}$	16 731.463	4.18×10^{-5}	3.02×10^{-5}
$^2{6_{06}}-{}^2{6_{16}}$	16 732.038	3.34×10^{-5}	2.83×10^{-5}

[a] The oscillator strengths were determined from the spectrum plotted in Figure 3 and from the spectrum published in Figure 4 of Rahinov et al.[25] The rotational assignments are given as $^{F'}N'_{K'_aK'_c}-{}^{F''}N''_{K''_aK''_c}$ (see text for an explanation of the notation).

3.2. Determining Absolute Densities of the NH Radical. The NH radical was observed via transitions in the (0,0), (1,1), and (2,2) vibrational bands of the $A^3\Pi \leftarrow X^3\Sigma^-$ electronic transition around 340 nm.[54,55] The electronic band spectrum of NH at 336 nm consists mainly of transitions of the nine branches for which the selection rules $\Delta K = \Delta J = 0, \pm 1$ apply, because $A^3\Pi \leftarrow X^3\Sigma^-$ is a Hund's coupling case b to case b electronic transition. The other branches with $\Delta K \neq \Delta J$ are very weak, except at lower J where a transition from Hund's coupling case b to case a in the $A^3\Pi$ state occurs. Furthermore, for each value of K, the total angular momentum apart from electronic spin, there are three levels denoted as F_1, F_2, and F_3 due to spin−orbit coupling. The quantum numbers for the total angular momentum J of the three levels are $J = K + 1$ for the F_1 levels, $J = K$ for the F_2 levels, and $J = K - 1$ for the F_3 levels. The rotational branch is denoted as $\Delta J_{F'_i,F''_i}$, where F'_i and F''_i indicate the upper and lower state F level.[56]

In Figure 4, spectra are depicted measured at $z = 10$, 20, and 36 cm in N_2 plasmas with H_2 injected in the background of the reactor (Figures 4a, 4c, and 4e) and in N_2-H_2 plasmas (Figures 4b, 4d, and 4f). The measured spectra for both plasmas at $z = 10$ cm contain strong rotational lines in the (0,0), (1,1), and (2,2) vibrational bands of the $A^3\Pi \leftarrow X^3\Sigma^-$ electronic transition. The line positions are plotted as ticks in the upper parts of the figures. The line positions and rotational assignments have been reported in the literature by Brazier et al.[54] and were simulated using the ROTSPEC software package using the molecular parameters given by Brazier et al. At $z = 10$ cm, all strong transitions reported in the literature, up to the rotational level $J = 18$ in the $v = 2$ state, were observed in N_2 plasmas with H_2 injected in the background of the reactor. At the same position in a N_2-H_2 plasma, only transitions from rotational levels up to $J = 11$ were observed. At $z = 21$ and 36 cm, all of the transitions of the (2,2) band, except for two transitions from low J, have completely disappeared in expanding N_2 plasmas with H_2 injected in the background of the reactor. In N_2-H_2 plasmas, no transitions of the (2,2) band were observed at these positions. The clear presence of transitions in the (1,1) and (2,2)

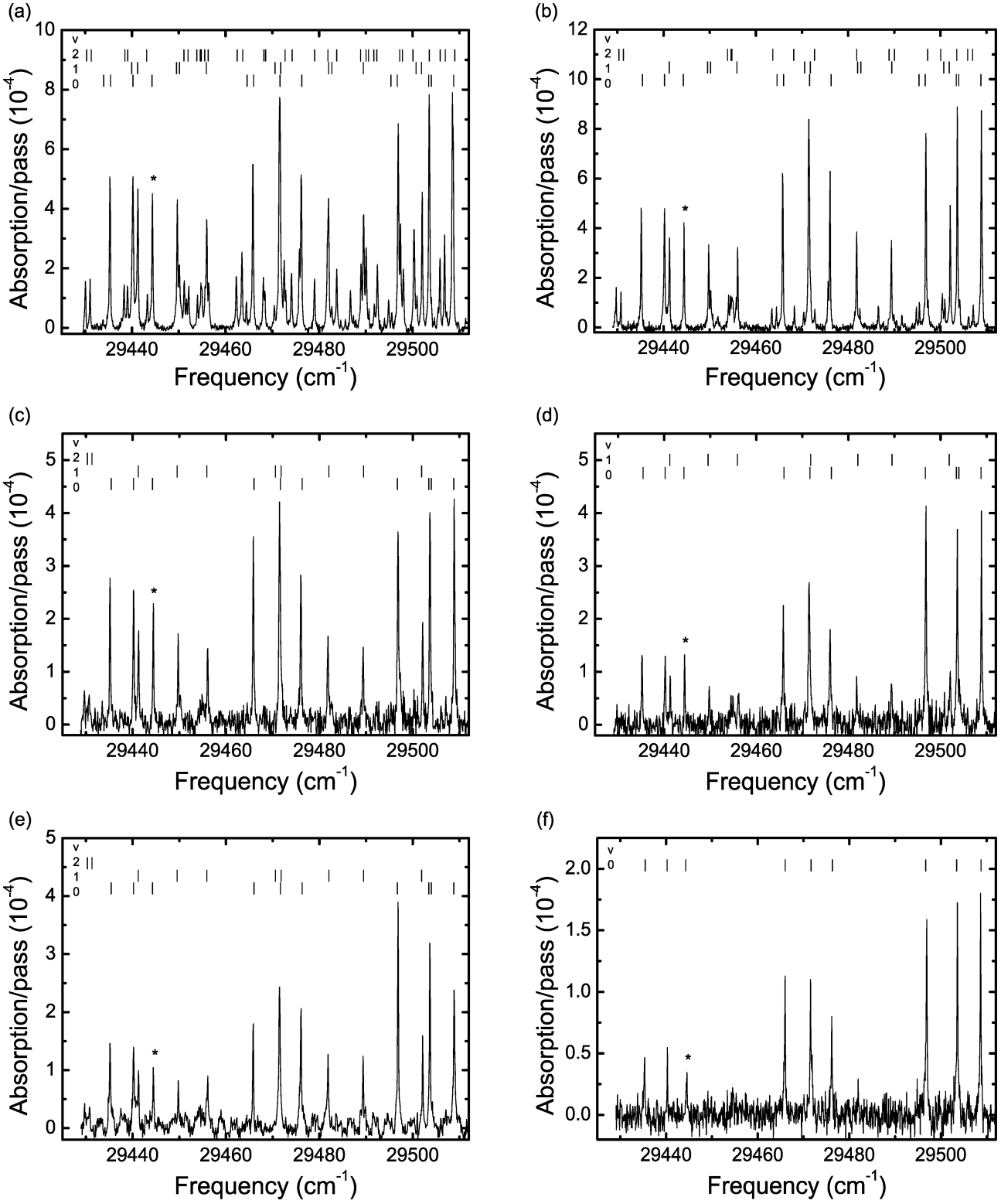

Figure 4. NH spectra as measured with cavity ring-down spectroscopy at $z = 10$ (a and b), 21 (c and d), and 36 cm (e and f). The plasma source was operated on 17 sccs N_2 while 5.56 sccs H_2 was injected in the background (parts a, c, and e) and on a mixture of 5 sccs N_2 and 11.67 sccs H_2 applied through the arc (parts b, d, and f). The arc current was 55 A, and the background pressure was 20 Pa. The line positions reported in the literature by Brazier et al.[54] and from the ROTSPEC software package are indicated by ticks in the upper part of the graph for the vibrational bands (0,0) (1,1), and (2,2). The "isolated'' $P_{33}(9)$ line at a center frequency of 29 444.28 cm^{-1} was used for the density measurements (marked by an asterisk).

bands indicates that the density distribution over the rotational and vibrational states are non-Boltzmann as will be discussed in more detail below.

The density of NH was determined by scanning the laser over the "isolated'' $P_{33}(9)$ line at a center frequency of 29 444.28 cm^{-1} (339.62 nm) (marked by an asterisk in Figure 4). The density of NH molecules in the lower state of the $P_{33}(9)$ transition was obtained using a value of the integrated absorption cross-section of $\sigma_{int} = 8.3 \times 10^{-21}$ m^2 cm^{-1}, which was calculated from the Einstein coefficient for spontaneous emission

calculated with information reported in the literature by Lents[55] and Schadee[57] (see ref 26). The total NH density was calculated by taking into account the density distribution over all possible states, which is determined by the kinetic, rotational, and vibrational temperatures of the NH radicals. The kinetic temperature of the NH radicals was again obtained from the Doppler broadening by deconvoluting the experimental absorption lines into a Lorentzian laser profile and a Gaussian Doppler contribution. This procedure yielded a laser line width of 0.11 $\pm$ 0.01 cm^{-1} at 29 444.28 cm^{-1}. The average NH kinetic gas temperature at the three positions from the plasma source proved to be the same as that for the NH_2 radicals, so 1775 $\pm$ 200 K at $z = 10$ and 21 cm from the plasma source and 1350 $\pm$ 250 K at $z = 36$ cm. As in the downstream plasma, all particles are collisionally coupled; the kinetic gas temperatures of the various particles are expected to be the same.

To determine how far the rotational density distribution could be characterized by a Boltzmann distribution, we extracted the rotational temperature of the NH radicals from a Boltzmann plot using the recorded spectra. The rotational density distribution at a temperature T_{rot} is given by

$$n(J) \propto (2J + 1) \exp(-E_{rot}(J)/kT_{rot}) \quad (4)$$

where $2J + 1$ is the statistical weight of the rotational level in the lower state, k is the Boltzmann constant, and $E_{rot}(J)$ is the energy of the rotational level in the lower state. The density $n(J)$ is given by

$$n(J) = A_{int}(J)/(\sigma_{int}(J)l) \quad (5)$$

where $A_{int}(J)$ is the integrated absorption of the measured transition, $\sigma_{int}(J)$ is the integrated absorption cross-section of the measured transition, and l is the absorption path length of the radicals in the plasma.

The densities in the various rotational levels $n(J)$ for the (0,0), (1,1), and (2,2) vibrational bands were determined using the integrated cross-sections derived from the Einstein coefficients for spontaneous emission. These were derived from the information reported in the literature by Lents[55] for the (0,0) and (1,1) bands[55] and from average of reported values in the literature as summarized by Seong et al. for the (2,2) band.[58] The complete derivation is given in ref 26.

A Boltzmann plot of the spectrum at $z = 10$ cm (Figure 4a) is shown in Figure 5, in which the statistically weighted densities $n(J)/(2J + 1)$ observed in an expanding N_2 plasma with H_2 injected in the background of the reactor are plotted as a function of the internal energy (rotational and vibrational). The low rotational levels in the three vibrational states were populated according to a Boltzmann distribution with $T_{rot} = 1775 \pm 80$ K. This value is equal to the kinetic temperature of the NH radicals. The density distribution in the low rotational levels indicates a thermalization of the radicals with the kinetic gas temperature by inelastic collisions with other particles. However, the high rotational levels, $J \geq 12$, in the $v = 2$ vibrational state were populated according to a temperature of 3430 $\pm$ 1300 K. This could also be true for the high rotational levels in other vibrational states, but transitions from these states were outside the measured spectral range. At $z = 20$ and 36 cm, the population of $v = 2$ is lower than the detection limit. Only two transitions from low J are observed but were too weak to determine the density in the $v = 2$ vibrational state. The NH radicals in these states have experienced enough collisions in the drift time to relax to rotational levels in the lower vibrational states. From the Boltzmann plots at $z = 20$ and 36 cm (Figure 6a), we concluded that the rotational temperature equals the kinetic gas temperature, i.e., 1775 K (at $z = 20$ cm) and 1350 K (at $z = 36$ cm).

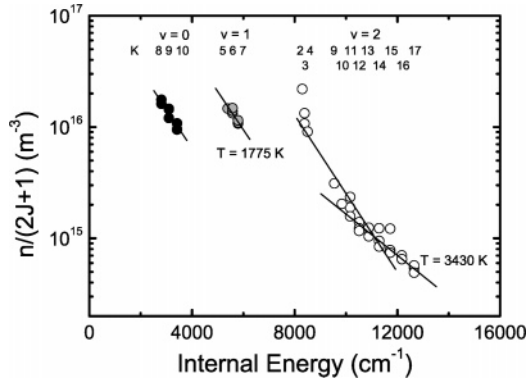

Figure 5. Statistically weighted densities $n(J)/(2J + 1)$ of the observed rotational levels at $z = 10$ cm in a N_2 plasma with H_2 injected in the background of the reactor as a function of the total internal energy (rotation and vibration). The spectrum is shown in Figure 4a. The plasma source was operated on 17 sccs N_2 while 5.56 sccs H_2 was injected in the background at an arc current of 55 A and a background pressure of 20 Pa. For $v = 2$, the rotational levels with $K > 12$ have a rotational temperature above the kinetic gas temperature.

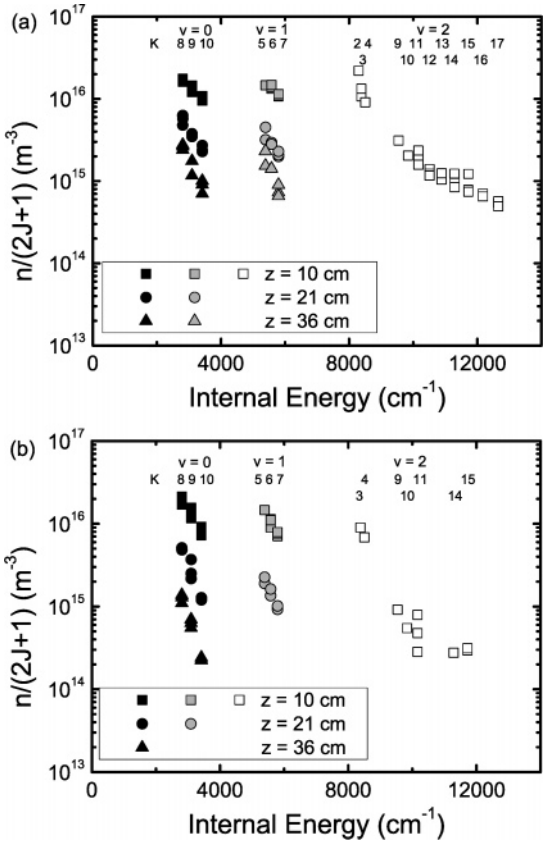

Figure 6. Statistically weighted densities $n(J)/(2J + 1)$ of the observed rotational levels at $z = 10$, 21, and 36 cm in N_2 plasmas with H_2 injected in the background of the reactor (on the left) and in expanding N_2-H_2 plasmas as a function of the total internal energy (rotation and vibration). The plasma source was operated on 17 sccs N_2 while 5.56 sccs H_2 was injected in the background and on a mixture of 5 sccs N_2 and 11.67 sccs H_2 at an arc current of 55 A. The background pressure was 20 Pa.

For the N_2-H_2 plasmas, we extracted from Boltzmann plots of the recorded spectra (Figure 6b) that the rotational levels in all vibrational states at all three positions from the plasma source were populated according to a rotational temperature equal to

the kinetic gas temperature at all three positions, even for the $v = 2$ band. It could be that the $v = 2$ band can also not be described with a single Boltzmann distribution in this case, but the measured spectral range contains not enough information to establish that.

That the rotational density distribution could be characterized by a Boltzmann distribution does not automatically imply that also the vibrational density distribution is a Boltzmann distribution. Because the energy spacing between the various vibrational levels is larger than the energy spacing between the rotational levels, the relaxation of the vibrational distribution to a Boltzmann distribution at the gas kinetic temperature takes more inelastic collisions and thus time. Therefore, first the total NH density in the vibrational states was calculated assuming a rotational Boltzmann distribution. The rotational Boltzmann fraction $f_{B,rot}$ for NH is taken from Herzberg[53]

$$f_{B,rot} = \frac{(2J+1)}{Q_r} \exp\left[-\frac{E_{rot}(K)}{kT_{rot}}\right] \quad (6)$$

where J is the quantum number of the total angular momentum of the lower level and Q_r is the rotational partition function. The partition functions Q_r can be approximated by the classical expression given by Herzberg.[53] For example, the total NH density (m^{-3}) in the (0,0) band at $z = 10$ cm can then be calculated using the integrated absorption A_{int} (cm^{-1}), an absorption path length of the radicals in the plasma $l = 0.1$ m, and $T = 1775$ K

$$n_{NH} = \frac{A_{int}}{\sigma_{int} l} \frac{1}{f_B} = (2.1 \pm 0.2) \times 10^{22} A_{int} \quad (7)$$

The complete derivation of the total density of NH in a vibrational state is given in ref 26.

From the distribution of the NH density over the vibrational states, we concluded that at all three positions in N_2 plasmas with H_2 injected in the background of the reactor the vibrational distribution is non-Boltzmann. Also in N_2-H_2 plasmas, the vibrational distribution is non-Boltzmann, except at $z = 36$ cm, where the total NH density distribution is in accordance with a Boltzmann distribution at 1350 K. We estimated the total density by adding the densities in the various vibrational states that we measured. In the following section, we show results of absolute densities of NH radicals as a function of the relative H_2 flow to the total H_2 and N_2 flow. We have assumed in the calculations of the total density that the distribution over the rovibrational energy levels at a certain position in the plasma expansion does not change significantly when the flows of H_2 and N_2 are changed.

3.3. Measured Trends in Absolute Densities of NH and NH_2 Radicals. We measured the trends in absolute densities of NH and NH_2 radicals for different relative N_2 and H_2 flows in two experimental situations: (1) expanding N_2 plasmas with H_2 injected in the background and (2) expanding N_2-H_2 plasmas in which both gases are fed through the plasma source.

3.3.1. N_2 Plasma with H_2 Injected in the Background. In the first experimental situation (Figure 1a), a plasma expansion was created from a pure N_2 flow of 17 sccs through the arc. The current through the arc was set at 55 A, and the downstream pressure was kept constant at 20 Pa by adjusting the gate valve to the pump. H_2 molecules were injected in the background of the reactor with a flow rate between 0 and 17 sccs. In Figure 7, the NH densities determined at three positions from the exit of the plasma source ($z = 10$, 21, 36 cm) are plotted as a function

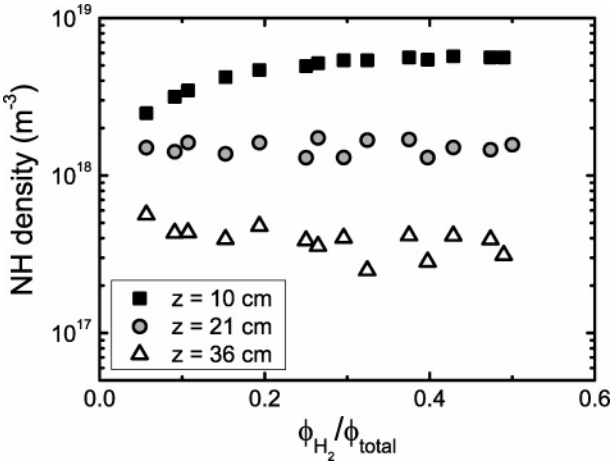

Figure 7. NH density as a function of the H_2 flow rate relative to the total flow rate of N_2 and H_2 measured by cavity ring-down spectroscopy. The plasma source was operated on 17 sccs N_2 at an arc current of 55 A, while a varying H_2 flow (0−17 sccs) was injected in the background. The background pressure was kept at 20 Pa.

of the H_2 flow rate, $\phi(H_2)$, relative to the total flow rate of N_2 and H_2 (ϕ(total)). The NH density increases with increasing relative H_2 flow and saturates at a level of $\sim 6 \times 10^{18}$ m^{-3} for relative H_2 flow rates larger than 0.25. From the recorded spectrum shown in section 3.2, the rotational and kinetic gas temperature has been determined to be around 1775 K (at $z =$ 10 and 21 cm) and 1350 K (at $z = 36$ cm). These temperatures are in agreement with previous measurements of temperatures of radicals produced in the plasma beam.[26,44] This indicates that in the case where H_2 is injected in the background of a N_2 plasma expansion the NH radicals are produced in the expansion. In this situation, no NH_2 was detected, which means that the NH_2 density is below our detection limit of $\sim 3 \times 10^{16}$ m^{-3}.

The flux density of the NH radicals in the plasma beam at $z = 10$ cm, assuming a velocity of 1000 m s^{-1},[30] is $\sim 6 \times 10^{21}$ m^{-2} s^{-1}. This gives a flow of NH radicals of $\sim 5 \times 10^{19}$ radicals s^{-1}, which corresponds to a flow of 2 sccs. It was previously determined that the N flux in pure N_2 plasma is $\sim$6 sccs.[30] This means that in the current situation 30% of the radical flux is NH.

3.3.2. N_2-H_2 Plasma. In the second experimental situation (Figure 1b), the plasma was produced from a mixture of N_2 and H_2 applied through the cascaded arc at a total flow of 17 sccs. Also during these experiments the current through the arc was 55 A, and the downstream pressure was kept constant at 20 Pa. The measured densities of NH and NH_2 as a function of $\phi(H_2)/\phi$(total) at $z = 10$, 21, and 36 cm are plotted in Figure 8. At all three positions, the NH density is almost constant at a level of $\sim 5 \times 10^{18}$ m^{-3} until a relative H_2 flow rate of about 0.5 and shows a slow decrease at higher relative H_2 flow rates. The NH_2 density increases with increasing $\phi(H_2)/\phi$(total) until $\phi(H_2)/\phi$(total) ≈ 0.85 and reaches at $z = 10$ cm an absolute maximum of $\sim 7 \times 10^{18}$ m^{-3}. Also in this situation the gas temperature, as determined from the recorded spectra shown in sections 3.1 and 3.2, is in agreement with previous measurements on radicals produced in the plasma beam.[26,44] In addition, no NH_2 was detected outside the plasma beam at a radial distance of 10 cm from the z-axis and at $z = 41.5$ cm. Both observations indicate that the NH_x radicals are produced in the plasma expansion.

The flux density of the NH_x radicals in the plasma beam at $z = 10$ cm is $\sim 1 \times 10^{22}$ m^{-2} s^{-1}, assuming that the velocity of the NH_x radicals is the same as that of the N radicals, i.e., 1000

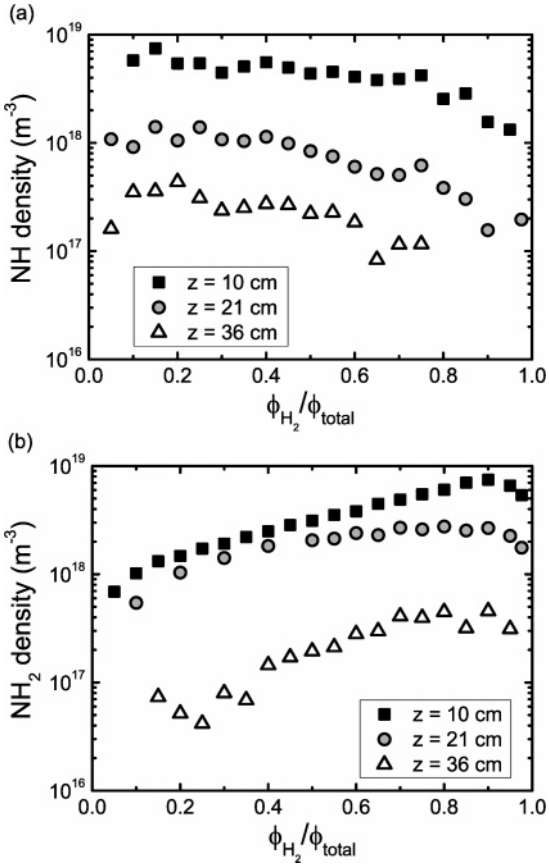

Figure 8. Densities of NH and NH_2 as a function of the H_2 flow rate relative to the total flow rate of N_2 and H_2 as measured by cavity ring-down spectroscopy at $z = 10$, 21, and 36 cm. Both N_2 and H_2 are applied through the arc at a total flow rate of 17 sccs at an arc current of 55 A. The background pressure was kept at 20 Pa.

m s^{-1}.[30] This gives a flow of NH_x radicals of about 1×10^{20} radicals s^{-1}, which corresponds to a flow of 4 sccs. This means that in the plasma expansion at $z = 10$ cm the NH and NH_2 radicals form about 60% of the radical flux.

In summary, the flux densities of the NH_x radicals with respect to the atomic radicals are in both experimental situations appreciable in the first part of the expansion. Further downstream in the expansion, densities of the NH_x radicals in both experimental situations decrease, mainly because of abstraction reactions, and some diffusion loss as will be addressed in the next section. At 36 cm from the exit of the plasma source, the densities of the NH_x radicals become smaller than those of the atomic radicals, whose density is $\sim 6 \times 10^{19}$ m^{-3} for N atoms[30] and 2×10^{19} m^{-3} for H atoms.[32] It can therefore be argued that at the reactor surfaces, i.e., outside the plasma expansion and in the downstream region, the N and H atoms play key roles in the generation of N_2, H_2, and NH_3. This was also inferred from a detailed study of the ammonia generation in N_2-H_2 plasmas.[10]

The highest efficiency of NH_3 production is reached if both N_2 and H_2 are flowing through the cascaded arc. The NH_3 density under those experimental conditions is about an order of magnitude higher than when N_2 is flowing through the arc and H_2 is injected in the background. For both types of plasmas, the NH_3 density is plotted as a function of the H_2 flow rate relative to the total flow rate in Figure 9. In the next section, the role of the NH_3 molecules in the production of the NH_x radicals will be shown.

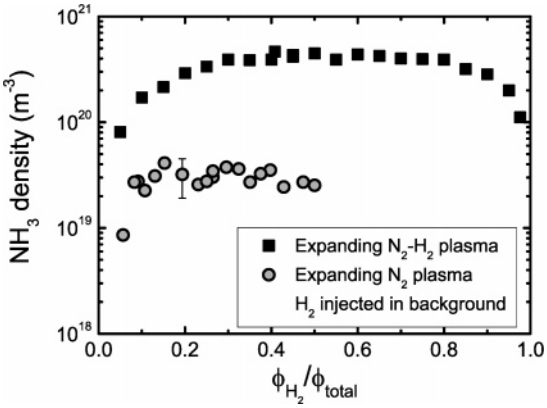

Figure 9. NH_3 density as measured in the background of the plasma reactor with mass spectrometry as a function of the relative H_2 flow rate for two different experimental situations. In the first experiment, N_2 is applied through the arc at a flow rate of 17 sccs, while H_2 is injected into the background of the reactor. In the second experiment, both N_2 and H_2 are applied through the arc at a total flow rate of 17 sccs. In both cases, the arc current was 55 A, and the background pressure was kept constant at 20 Pa.

4. Discussion

We will now discuss the production mechanisms of the NH and NH_2 radicals under both plasma conditions. It will be argued that the roles of metastable N atoms and of metastable nitrogen molecules can be neglected under our experimental conditions and that the main chemistry in which the NH_x radicals are produced is induced by ground state N and H atoms and, although to a much lower extent, atomic nitrogen ions. Also, the importance of the presence of NH_3 molecules, formed in the plasma reactor, will be addressed.

For a pure N_2 plasma, the densities of the metastable $N(^2P)$ and $N(^2D)$ atoms emanating from the plasma source are at maximum 20% of the $N(^4S)$ atoms (assuming a thermal population at a temperature of 1 eV in the plasma source). In the first few centimeters of the plasma expansion, the $N(^2P)$ and $N(^2D)$ densities will decrease mainly due to de-excitation by collisions with electrons ($k_e \approx 10^{-13}$ m^3 s^{-1}).[59] Next, the metastable atoms are de-excited by collisions with $N(^4S)$ atoms and N_2 molecules (rate constant of $4.1 \times 10^{-17} m^3$ s^{-1}).[30] These collisions are fast compared to reactions with H_2 molecules.[11] The same de-excitation mechanisms also apply to the $N(^2D)$ and $N(^2P)$ atoms generated in dissociative recombination of N_2^+ ions. The metastable atoms created in this way represent at maximum a few percent of the total flow (equal to the initial N^+ flow).

The ionization degree of a plasma expansion of pure N_2 under similar experimental conditions has been determined in ref 30. At the nozzle outlet, i.e., at $z = 0.2$ cm, the electron density was measured to be 10^{20} m^{-3}, which corresponded to an ionization degree of $\sim$1%. In the supersonic part, the electron density decreased with $1/z^2$ and was $\sim 4 \times 10^{18}$ m^{-3} behind the stationary shock (at $z = 2.5$ cm) in the subsonic region. At 20 Pa, this means that the ionization degree behind the shock is less than 3×10^{-3}.

In most nitrogen-containing plasma, N_2 molecules in the $A^3\Sigma_u^+$ state are considered to be important for the plasma chemistry. At the exit of our plasma source, the density of $N_2(A^3\Sigma_u^+)$ molecules is less than 1% of the density of $N_2(X)$ molecules, i.e., $N_2(A)/N_2(X) \leq 10^{-2}$ and will decrease fast via electron collisions and by with N atoms.[60] Previously, metastable $N_2(A^3\Sigma_u^+)$ molecules have been observed in expanding pure N_2

plasmas; it was assumed that they were produced by surface association of N atoms. This observation was made in a low-current, low-flow N_2 plasma with a very low ionization degree (less than 10^{-3}). Due to the low N^+ density, the $N_2(A)$ density is high. At high N^+ density, a very efficient loss channel for $N_2(A^3\Sigma_u^+)$ molecules exists, i.e., resonant charge transfer to N_2^+. In the plasma conditions discussed here, a higher ion density than in the low-flow, low-current experiments was present, and the $N_2(A^3\Sigma_u^+)$ molecules are efficiently lost by the charge-transfer reaction.[61]

We thus conclude that in the plasma expansions discussed here the main neutral chemistry is initiated by $N(^4S)$ atoms. Although the ionization degree is very low, reactions with N^+ ions need to be considered due to the large cross-sections for charge-transfer collisions as compared to van der Waals collisions. This will be treated separately for each plasma condition.

As mentioned in section 3.3, in both plasma conditions appreciable amounts of NH_3 are formed in the background. To elucidate the possible role of NH_3 molecules in the plasma chemistry leading to NH_x radicals, we will first summarize the results of a previous study on the production of NH and NH_2 radicals in an Ar-plasma expansion to which NH_3 was added in the background.[26] From that study, we concluded that in the presence of Ar^+ ions the charge-transfer reaction

$$Ar^+ + NH_3 \rightarrow Ar + NH_3^+ \tag{8}$$

with subsequent dissociative recombination of the molecular ion with electrons was the most important source of NH radicals and could partially explain the observed NH_2 densities

$$NH_3^+ + e \rightarrow NH + 2H$$
$$\rightarrow NH_2 + H \tag{9}$$

with a rate constant of 2×10^{-13} m^3 s^{-1} for an electron temperature around $\hat{T}_e = 0.3$ eV.[29,33] Furthermore, we determined that the branching ratio of the dissociative recombination reaction of NH_3^+ is for 80% to NH and 20% to NH_2. It was also shown that the reactions

$$NH_3^+ + NH_3 \rightarrow NH_4^+ + NH_2 \tag{10}$$

and

$$NH_3 + H \rightarrow NH_2 + H_2 \tag{11}$$

play a significant role in the production of NH_2 radicals. The latter has a rather low rate constant of 4×10^{-18} m^3 s^{-1} at a temperature of 1750 K due to an activation energy of 4991 K,[62] and the observed NH_2 densities could only be explained if the reaction rate was increased by a factor of 7.5 to 2.5×10^{-17} m^3 s^{-1}. This increase could be ascribed to the presence of energetic H atoms in the plasma. The dependence of the reaction rate on the kinetic energy of the particles involved is generally known for ion−molecule reactions. Studies on the kinetic energy dependence of endothermic charge-transfer reactions have shown that, with increasing ion kinetic energy, these reaction channels become available.[63,64] A similar enhancement of the reaction rate might occur during neutral−neutral collisions.

In the present experiments, the plasmas are created from mixtures of N_2 and H_2 (either injected in the plasma source or downstream in the plasma expansion) instead of injected NH_3. However, also in these plasmas a significant amount of background gas in the reactor is ammonia (Figure 9). The ammonia will diffuse into the plasma beam, and except for the role of the Ar^+ ions, which is now taken over by the N^+ ions, similar reaction paths will be active. Furthermore, in these plasmas also reactions involving H atoms and H_2 molecules as well as N atoms need to be considered (vide infra).

4.1. N_2 Plasma with H_2 Injected in the Background. In the case where the plasma expansion is produced from pure nitrogen and H_2 molecules are injected into the background, the H_2 molecules can diffuse into the expanding plasma beam and can be dissociated by N^+ ions emanating from the plasma source via charge transfer followed by dissociative recombination[65]

$$N^+ + H_2 \rightarrow NH^+ + H \tag{12}$$

$$NH^+ + e \rightarrow N + H \tag{13}$$

The rate constants for reactions 12 and 13 are 5.4×10^{-16} and 2×10^{-13} m^3 s^{-1}, respectively. Vankan et al.[9] proposed this dissociation mechanism for the H_2 molecules to explain the trends in the production of NH_3 measured as a function of the H_2 flow injected into the background of a pure nitrogen plasma expansion. However, because in these reactions no molecular radicals are formed, other reactions have to be included to explain the trends in the densities of the NH_x radicals. One possible other reaction could be

$$N^+ + H_2 \rightarrow NH + H^+ \tag{14}$$

To the best of our knowledge, no value for the reaction rate is reported. As the reaction is resonant, we will assume that it has a rate constant of 5.4×10^{-16} m^3 s^{-1} similar to that of reaction 12. However, already from a comparison between a calculation of the flux of NH radicals that can be produced via reaction 14 and the measured NH flux at $z = 10$ cm, we conclude that this reaction channel cannot be the main production channel for NH. If we assume a velocity of 1000 m s^{-1} for the particles in the beam at $z = 10$ cm, then the measured flux of NH at that position is 2 sccs for $\phi(H_2)/\phi(\text{total}) > 0.2$ (assuming a 10 cm radius for the plasma beam). Because we know that the ionization degree at the exit of the arc is not more than 1%,[30] a maximum flow of 0.3 sccs of ions enters the reactor (at a total N_2 flow of 17 sccs). Via reaction 14 this can result in a maximum flow of 0.3 sccs of NH. To explain the measured total NH flux of 2 sccs, we propose that the following reaction has to be taken into account

$$N + H_2 \rightarrow NH + H$$
$$k = 3.9 \times 10^{-16} \exp\left(\frac{-15\,775}{T}\right) m^3\ s^{-1} \tag{15}$$

Due to its high activation energy of 15 775 K,[65] the rate constant at 1775 K is rather low, i.e., 5.3×10^{-20} m^3 s^{-1}. With this rate constant and a density of atomic nitrogen in the plasma expansion of $\sim 1 \times 10^{20}$ m^{-3},[30] this reaction cannot fully explain the observed NH density. However, the rate of reaction 15 will be higher in the supersonic expansion region and the first part of subsonic expansion, where H_2 molecules can diffuse into the plasma expansion. There N atoms with kinetic energies in excess of 0.5−1 eV are expected.[30] Namely, thermal energies of a few thousand kelvin are possible in the first few centimeters after the shock. Also substantial rotational−vibrational excitation of $H_2^{(r,v)}$ molecules has been observed.[32,66] We therefore assume that in total approximately 1 eV of energy is available to the

TABLE 2: Reactions and Rate Constants

no.	reaction			rate constant ($m^3 s^{-1}$)	reference
R1	$N^+ + NH_3$	→	$N + NH_3^+$	2×10^{-15}	64
		→	$HN_2^+ + H_2$	2.2×10^{-16}	
		→	$H_2N^+ + NH$	2.2×10^{-16}	
R2	$N^+ + H_2$	→	$NH^+ + H$	5.4×10^{-16}	64
		→	$NH + H^+$	$\approx 5 \times 10^{-16}$ [a]	
R3	$NH_3^+ + e$	→	$NH_2 + H$	3.6×10^{-14} [b]	
		→	$NH + 2H$	1.4×10^{-13}	
R4	$NH^+ + e$	→	$N + H$	2×10^{-13}[b]	
R5	$HN_2^+ + e$	→	$NH + N$	2.6×10^{-14}	70
		→	$H + N_2$	1.4×10^{-14}	
R6	$H_2N^+ + e$	→	$H_2 + N$	2×10^{-13} [b]	
R7	$N + H_2$	→	$NH + H$	3.9×10^{-16} for $z < 10$ cm[c]	
				$3.9 \times 10^{-16} \exp((-250z)/T)$ for $z > 10$cm	
R8	$NH + H$	→	$N + H_2$	$8.3 \times 10^{-17} \exp(-1000/T)$	64
R9	$NH + N$	→	$N_2 + H$	$1.8 \times 10^{-17}(T/300)^{0.5}$	64
R10	$NH + NH$	→	$N + NH_2$	$1.7 \times 10^{-18}(T/300)^{0.5} \exp(-10000/T)$[c]	
R11	$NH_2 + H$	→	$NH + H_2$	3.2×10^{-17}	64
R12	$N + NH_2$	→	$N_2 + 2H$	1.2×10^{-16}	10
R13	$N + NH_2$	→	$NH + NH$	$4 \times 10^{-17}(T/300)^{0.5}$ for $z < 10$ cm[c]	
				$4 \times 10^{-17}(T/300)^{0.5} \exp((-250 \times z)/T)$ for $z > 10$ cm	
R14	$NH_3 + H$	→	$NH_2 + H_2$	2.5×10^{-17}	25

[a] Estimated rate constant for charge-transfer reactions as no information is available in the literature. [b] Estimated rate constant for dissociative recombination reactions. [c] Rate constant as determined in this paper.

particles involved in the reaction, which would give a rate constant of 4×10^{-16} m^3 s^{-1} for $z < 10$ cm. As a consequence of the above, also other reactions involving N atoms have a higher rate constant. For example, also the rate constant of the reaction between N atoms and NH_2[65]

$$N + NH_2 \rightarrow NH + NH$$

$$k = 4 \times 10^{-17}\left(\frac{T}{300}\right)^{0.5} \exp\left(\frac{-11\,890}{T}\right) \text{m}^3\,\text{s}^{-1} \quad (16)$$

becomes substantially higher, i.e., a rate constant of 1×10^{-16} m^3 s^{-1} for $z < 10$ cm. In Table 2, the final expression for the rate constants of reactions 15 and 16 as a function of z are given, reactions R7 and R13.

It is observed that the NH density has a maximum at $z = 10$ cm and decreases further downstream. This is partly caused by the loss of NH radicals due to diffusion out of the plasma beam. The main loss channel of NH radicals is abstraction reactions with N and H atoms or by reactions between two NH radicals, resulting in N_2 and H_2 molecules and N and H atoms (reactions R8−R13) (Table 2). By calculating the NH density using the reactions and rate constants given in ref 64, the obtained NH_2 density is more than one order above the detection limit. Because no NH_2 was observed, the activation energy of the reaction between two NH radicals[65]

$$NH + NH \rightarrow NH_2 + H$$

$$k = 5.8 \times 10^{-18}\left(\frac{T}{300}\right)^{0.5} \exp\left(\frac{-1000}{T}\right) \text{m}^3\,\text{s}^{-1} \quad (17)$$

should be increased. As E_a is assumed to be 10 000 K, the rate constant becomes 5×10^{-20} m^3 s^{-1} (reaction R10 in Table 2). Using this rate constant, the calculated NH_2 density is below our detection limit of $\sim 3 \times 10^{16}$ m^{-3}.

4.2. N_2-H_2 Plasma. In the case of an expanding N_2-H_2 plasma, the gas mixture of N_2 and H_2 is almost fully dissociated in the plasma source. However, inside the nozzle the hydrogen and nitrogen atoms will partially recombine at the surface, leading to (rovibrationally excited) molecules.[10,66] This loss mechanism is less important for nitrogen atoms than for hydrogen atoms, because the association rate for nitrogen atoms is lower than that for hydrogen atoms. The loss probability of H atoms on copper surfaces is reported in literature to be 0.3−0.5,[67,68] whereas values for N atoms vary from 3.9×10^{-2} to 8.5×10^{-4}.[69,70] The amount of ions emanating from the plasma source is very low (less than 1%), and we assume the ratio of the fluxes of N^+ and H^+ exiting the arc to be equal to the ratio of N_2 and H_2 in the gas mixture flowing through the arc. Although the H_2 molecules are in this case injected in the arc, the maximum flux of NH radicals can be calculated in the same way as for the previous plasma condition. At the low relative H_2 flow, the flux of N^+ exiting the source and the NH flux at $z = 10$ cm are the same as in the previous situation; also now reaction 14 can only account for 15% of the measured NH flux. Furthermore, the NH flux would linearly decrease with increasing $\phi(H_2)/\phi(\text{total})$, while up to $\phi(H_2)/\phi(\text{total}) \approx 0.75$ the NH flux is measured to be constant (Figure 8). So also in this plasma condition reaction 15 has to taken into account. The hydrogen molecules can both originate from the injected H_2 flow but also from hydrogen molecules formed in the plasma reactor (and like in the previous case diffuse into the plasma beam). However, we know that there is also NH_3 present in the background, which will diffuse into the plasma beam and react with N^+ ions and H atoms (reaction 11). The N^+ reaction channel will not be very important, because the reaction with H_2 molecules, from both the plasma expansion and the background, will be much more effective than with NH_3 diffusing into the beam. We therefore propose the neutral-dominated reaction path (reaction 11) for the NH_x radical production. When more H_2 is added to the gas mixture, more NH_2 radicals are produced by reactions between H atoms and NH_3 molecules, followed by the reaction between H and NH_2 leading to NH (reactions R14 and R11 in Table 2). This is underpinned by the stronger increase of NH_2 compared to the trend of ammonia in Figure 9 and by the fact that the maximum NH_2 density is observed at high hydrogen flows.

It is observed that the NH density has its maximum at $z = 10$ cm and decreases further downstream. The NH densities as a function of the relative H_2 flow show the same H_2 dependence at the three positions in the plasma beam. Furthermore, the

gradient of the NH density as a function of the measured position in the plasma beam has a constant factor of about 5 between positions. Both observations suggest that the loss mechanism of NH is the same for all three positions measured. We ascribe the loss of NH radicals partly to diffusion out of the plasma beam but mainly to abstraction reactions with N and H atoms or by reactions between two NH radicals, reactions R8−R13 (Table 2).

The gradient of the NH_2 density as a function of the measured position in the plasma beam gives a factor of 2 between $z = 10$ and 20 cm, whereas it is a factor 10 between $z = 21$ and 36 cm. That this factor is not constant as it is in the case of NH can be explained as follows. The NH_2 radicals are produced in a reaction between H atoms and NH_3 molecules, which also still can take place after $z = 10$ cm. Thus, in contrast to the NH radicals, the NH_2 radicals are still produced after $z = 10$ cm. This counteracts the loss of NH_2 radicals due to diffusion out of the plasma beam of the radicals and by abstraction reactions with H atoms. After $z = 21$ cm, the density of the NH_2 radicals is determined by these processes as almost no production occurs.

5. Conclusions

To determine the production mechanisms of NH and NH_2 radicals in expanding N_2 plasmas to which H_2 was added in the background and in expanding N_2-H_2 plasmas, we measured the density evolution of these radicals along the expansion axis by means of cavity ring-down spectroscopy. The NH radical was observed via transitions in the (0,0), (1,1), and (2,2) vibrational bands of the $A^3\Pi \leftarrow X^3\Sigma^-$ electronic transition and the NH_2 radical via transitions in the (0,9,0) ← (0,0,0) band of the $\tilde{A}^2A_1 \leftarrow \tilde{X}^2B_1$ electronic transition. From the measured NH_2 spectrum, we determined the oscillator strengths of part of the transitions in the $^PQ_{1,N}$ branch of the Σ vibronic sub-band.

From the density distribution of the rotational states of the NH radical in an expanding N_2 plasma with H_2 injected in the background, we concluded that the low rotational levels in the three vibrational states were populated according to a Boltzmann distribution. However, at $z = 10$ cm the high rotational levels, $J \geq 12$, in the $v = 2$ vibrational state were overpopulated. At the other two positions, only two rotational transitions in $v = 2$ were observed. In N_2-H_2 plasmas, the rotational levels in all vibrational states were populated according to a Boltzmann distribution at the three positions in the plasma expansion.

From the distribution of the NH densities over the vibrational states, we concluded that at all three positions in both types of plasmas the vibrational distribution deviated from a Boltzmann distribution, except at $z = 36$ cm in N_2-H_2 plasmas.

The measurements revealed typical densities of 5×10^{18} m^{-3} for the NH radical in both plasmas and up to 7×10^{18} m^{-3} for the NH_2 radical when H_2 and N_2 are both fed through the plasma source. In N_2 plasma with H_2 injected in the background, no NH_2 was detected, indicating that the density is below our detection limit of 3×10^{16} m^{-3}. In N_2 plasma with H_2 injected in the background, the flux density of the NH radicals in the plasma beam at $z = 10$ cm is about 6×10^{21} m^{-2} s^{-1}. This corresponds to a flow of 2 sccs, and this means that in this plasma 30% of the radical flux is NH. In N_2-H_2 plasma, the flux density of the NH_x radicals in the plasma beam at $z = 10$ cm is about 1×10^{22} m^{-2} s^{-1}. This corresponds to a flow of 4 sccs, and this means that in N_2-H_2 plasma at $z = 10$ cm the NH and NH_2 radicals form about 60% of the radical flux. The flux densities of the NH_x radicals with respect to the atomic radicals are appreciable in the first part of the expansion. Further downstream the NH_x radicals are dissociated, and their densities become smaller than those of the atomic radicals. It is concluded that the NH_x radicals play an important role as precursors for the N and H atoms, key to the surface production of N_2, H_2, and NH_3 molecules.

In both plasmas that have been studied, the NH_x radicals are produced in the plasma expansion. The results of expanding N_2 plasmas to which H_2 was added in the background point to a formation of NH by a reaction between N atoms emitted by the plasma source and H_2 molecules with a minor contribution from the reaction of N^+ with H_2. In expanding N_2-H_2 plasmas, two mechanisms are responsible for the production of NH radicals. The NH production occurs in the same way as mentioned above, thus via N and H_2. But NH is also formed by abstraction from NH_2, which is in turn formed in a reaction between H and NH_3. That NH_2 was not detected in the case where H_2 is added to a N_2 plasma indicates that in this plasma reactions involving NH_3 play no significant role in the production of NH_x radicals.

Acknowledgment. The authors acknowledge C. C. H. Lamers for her contribution during the measurements of the NH radicals, G. Yagci for the NH_3 measurements, and M. J. F. van de Sande, J. F. C. Jansen, A. B. M. Hüsken, and H. M. M. de Jong for their technical assistance. This work is part of the research program of the Foundation for Fundamental Research on Matter (FOM), which is financially supported by the Netherlands Organization for Scientific Research (NWO) and by the Netherlands Ministry of Economic Affairs, the Ministry of Education, Culture, and Science and the Ministry of Public Housing, Physical Planning, and Environment (EET project "HR-CEL''). The research of one of the authors (W.K.) has been made possible by a fellowship of the Royal Netherlands Academy of Arts and Sciences (KNAW).

References and Notes

(1) Ricard, A.; Gordiets, B. F.; Pinheiro, M. J.; Ferreira, C. M.; Baravian, G.; Amorim, J.; Bockel, S.; Michel, H. *Eur. Phys. J.: Appl. Phys.* **1998**, *4*, 87.

(2) Kessels, W. M. M.;van Assche, F. J. H.; Hong, J.; Schram, D. C.; van de Sanden, M. C. M. *J. Vac. Sci. Technol., A* **2004**, *22*, 96.

(3) Kim, H. *J. Vac. Sci. Technol., B* **2003**, *21*, 2231.

(4) Heil, S. B. S.; Langereis, E.; Roozeboom, F.; van de Sanden, M. C. M.; Kessels, W. M. M. *J. Electrochem. Soc.* **2006**, *153*, G956.

(5) Nagai, H.; Hiramatsu, M.; Hori, M.; Goto, T. *J. Appl. Phys.* **2003**, *94*, 1362.

(6) Eremin, E. N. *Russ. J. Phys. Chem.* **1975**, *49*, 1112.

(7) Uyama, H.; Matsumoto, O. *Plasma Chem. Plasma Process.* **1989**, *9*, 13.

(8) Yin, K. S.; Venugopalan, M. *Plasma Chem. Plasma Process.* **1983**, *3*, 343.

(9) Vankan, P.; Rutten, T.; Mazouffre, S.; Schram, D. C.; Engeln, R. *Appl. Phys. Lett.* **2002**, *81*, 418.

(10) van Helden, J. H.; Wagemans, W.; Zijlmans, R. A. B.; Schram, D. C.; Engeln, R.; Lombardi, G.; Stancu, G. D.; Röpcke, J. *J. Appl. Phys.* **2007**, *101*, 043305.

(11) Gordiets, B.; Ferreira, C. M.; Pinheiro, M. J.; Ricard, A. *Plasma Sources Sci. Technol.* **1998**, *7*, 363.

(12) Gordiets, B.; Ferreira, C. M.; Pinheiro, M. J.; Ricard, A. *Plasma Sources Sci. Technol.* **1998**, *7*, 379.

(13) Jauberteau, J. L.; Jauberteau, I.; Aubreton, J. *J. Phys. D: Appl. Phys.* **2002**, *35*, 665.

(14) Amorim, J.; Baravian, G.; Ricard, A. *Plasma Chem. Plasma Process.* **1995**, *15*, 721.

(15) Bockel, S.; Amorim, J.; Baravian, G.; Ricard, A.; Stratil, P. *Plasma Sources Sci. Technol.* **1996**, *5*, 567.

(16) Fisher, E. R.; Ho, P.; Breiland, W. G.; Buss, R. J. *J. Phys. Chem.* **1992**, *96*, 9855.

(17) McCurdy, P. R.; Butoi, C. I.; Williams, K. L.; Fisher, E. R. *J. Phys. Chem. B* **1999**, *103*, 6919.

(18) Steen, M. L.; Kull, K. R.; Fisher, E. R. *J. Appl. Phys.* **2002**, *92*, 55.

(19) Uyama, H.; Matsumoto, O. *Plasma Chem. Plasma Process.* **1989**, *9*, 421.
(20) Kiyooka, H.; Matsumoto, O. *Plasma Chem. Plasma Process.* **1996**, *16*, 547.
(21) Halpern, J. B.; Hancock, G.; Lenzi, M.; Welge, K. H. *J. Chem. Phys.* **1975**, *63*, 4808.
(22) Rahinov, I.; Ditzian, N.; Goldman, A.; Cheskis, S. *Appl. Phys. B: Lasers Opt.* **2003**, *77*, 541.
(23) Derzy, I.; Lozovsky, V. A.; Ditzian, N.; Rahinov, I.; Cheskis, S. *Proc. Combust. Inst.* **2000**, *28*, 1741.
(24) Friedrichs, G.; Colberg, M.; Fikri, M.; Huang, Z.; Neumann, J.; Temps, F. *J. Phys. Chem. A* **2005**, *109*, 4785.
(25) Rahinov, I.; Goldman, A.; Cheskis, S. *Appl. Phys. B: Lasers Opt.* **2005**, *81*, 143.
(26) van den Oever, P. J.; van Helden, J. H.; Lamers, C. C. H.; Engeln, R.; Schram, D. C.; van de Sanden, M. C. M.; Kessels, W. M. M. *J. Appl. Phys.* **2005**, *98*, 093301.
(27) van den Oever, P. J.; van Hemmen, J. L.; van Helden, J. H.; Schram, D. C.; Engeln, R.; van de Sanden, M. C. M.; Kessels, W. M. M. *Plasma Sources. Sci. Technol.* **2006**, *15*, 546.
(28) van den Oever, P. J.; van Helden, J. H.; van Hemmen, J. L.; Engeln, R.; Schram, D. C.; van de Sanden, M. C. M.; Kessels, W. M. M. *J. Appl. Phys.* **2006**, *100*, 093303.
(29) (a) van de Sanden, M. C. M.; Severens, R. J.; Kessels, W. M. M.; Meulenbroeks, R. F. G.; Schram, D. C. *J. Appl. Phys.* **1998**, *84*, 2426. (b) van de Sanden, M. C. M.; Severens, R. J.; Kessels, W. M. M.; Meulenbroeks, R. F. G.; Schram, D. C. *J. Appl. Phys.* **1999**, *85*, 1243.
(30) Mazouffre, S.; Bakker, I.; Vankan, P.; Engeln, R.; Schram, D. C. *Plasma Sources Sci. Technol.* **2002**, *11*, 439.
(31) Dahiya, R. P.; de Graaf, M. J.; Severens, R. J.; Swelsen, H.; van de Sanden, M. C. M.; Schram, D. C. *Phys. Plasmas* **1994**, *1*, 2086.
(32) Vankan, P.; Schram, D. C.; Engeln, R. *Plasma Sources Sci. Technol.* **2005**, *14*, 744.
(33) van de Sanden, M. C. M.; de Regt, J. M.; Jansen, G. M.; van der Mullen, J. A. M.; Schram, D. C.; van der Sijde, B. *Rev. Sci. Instrum.* **1992**, *63*, 3369.
(34) Meulenbroeks, R. F. G.; van Beek, A. J.; van Helvoort, A. J. G.; van de Sanden, M. C. M.; Schram, D. C. *Phys. Rev. E* **1994**, *49*, 4397.
(35) Engeln, R.; Mazouffre, S.; Vankan, P.; Schram, D. C.; Sadeghi, N. *Plasma Sources Sci. Technol.* **2001**, *10*, 595.
(36) Vankan, P.; Mazouffre, S.; Engeln, R.; Schram, D. C. *Phys. Plasmas* **2005**, *12*, 102303.
(37) *Cavity-Ringdown Spectroscopy: An Ultratrace-Absorption Measurement Technique*; Busch, K. W., Busch, M. A., Eds.; ACS Symposium Series 720; American Chemical Society: Washington, DC, 1999.
(38) Vankan, P. J. W. Ph.D. Thesis, Eindhoven University of Technology, Eindhoven, The Netherlands, 2005. http://alexandria.tue.nl/extra2/200510358.pdf.
(39) Mazouffre, S.; Vankan, P.; Engeln, R.; Schram, D. C. *Phys. Plasmas* **2001**, *8*, 3824.
(40) Boogaarts, M. G. H.; Böcker, P. J.; Kessels. W. M. M.; Schram, D. C.; van de Sanden, M. C. M. *Chem. Phys. Lett.* **2000**, *326*, 400.
(41) Kessels, W. M. M.; Leroux, A.; Boogaarts, M. G. H.; Hoefnagels, J. P. M.; van de Sanden, M. C. M.; Schram, D. C. *J. Vac. Sci. Technol., A.* **2001**, *19*, 467.
(42) Mazouffre, S.; Boogaarts, M. G. H.; Bakker, I. S. J.; Vankan, P.; Engeln, R.; Schram, D. C. *Phys. Rev. E* **2001**, *64*, 016411.
(43) Brussaard, G. J. H. Ph.D. Thesis, Eindhoven University of Technology, Eindhoven, The Netherlands, 1999. http://alexandria.tue.nl/extra2/9900312.pdf.
(44) Hoefnagels, J. P. M.; Barrell, Y.; Kessels, W. M. M.; van de Sanden, M. C. M. *J. Appl. Phys.* **2004**, *96*, 4094.
(45) *TU/eDACS*; Technical Laboratory Automation Group, Eindhoven University of Technology: Eindhoven, The Netherlands.
(46) Dressler, K.; Ramsay, D. A. *Philos. Trans. R. Soc. London, Ser. A* **1959**, *251*, 553.
(47) Ross, S. C.; Birss, F. W.; Vervloet, M.; Ramsay, D. A. *J. Mol. Spectrosc.* **1988**, *129*, 436.
(48) Kohse-Höinghaus, K.; Davidson, D. F.; Chang, A. Y.; Hanson, R. K. *J. Quant. Spectrosc. Radiat. Transfer* **1989**, *42*, 1.
(49) Votsmeier, M.; Song, S.; Davidson, D. F.; Hanson, R. K. *Int. J. Chem. Kinet.* **1999**, *31*, 323.
(50) *PrecisionScan-D Dye Laser Manual*; Sirah Laser- und Plasmatechnik GmbH: Darmstadt, Germany, 1999.
(51) Mazouffre, S. Ph.D. Thesis, Eindhoven University of Technology, Eindhoven, The Netherlands, 2001. http://alexandria.tue.nl/extra2/200142219.pdf.
(52) Green, R. M.; Miller, J. A. *J. Quant. Spectrosc. Radiat. Transfer* **1981**, *26*, 313.
(53) Herzberg, G. *Molecular Spectra and Molecular Structure*; Van Nostrand: New York, 1964; Vol. 2.
(54) Brazier, C. R.; Ram, R. S.; Bernath, P. F. *J. Mol. Spectrosc.* **1986**, *120*, 381.
(55) Lents, J. M. *J. Quant. Spectrosc. Radiat. Transfer* **1973**, *13*, 297.
(56) Herzberg, G. *Molecular Spectra and Molecular Structure*; Van Nostrand: New York, 1964; Vol. 1.
(57) Schadee, A. *Astron. Astrophys.* **1975**, *41*, 213.
(58) Seong, J.; Park, J. K.; Sun, H. *Chem. Phys. Lett.* **1994**, *228*, 443.
(59) Van, der Mullen, J. A. M. *Phys. Rep.* **1990**, *191*, 110.
(60) Cernogora, G.; Ferreira, C. M.; Hochard, L.; Touzeau, M.; Loureiro, J. *J. Phys. B: At., Mol. Opt. Phys.* **1984**, *17*, 4429.
(61) Brussaard, G. J. H.; Aldea, E.; van de Sanden, M. C. M.; Dinescu, G.; Schram, D. C. *Chem. Phys. Lett.* **1998**, *290*, 379.
(62) Ko, T.; Marshall, P.; Fontijn, A. *J. Phys. Chem.* **1990**, *94*, 1401.
(63) Weber, M. E.; Armentrout, P. B. *J. Chem. Phys.* **1989**, *90*, 2213.
(64) Armentrout, P. B. *J. Anal. At. Spectrom.* **2004**, *19*, 571.
(65) Capitelli, M.; Ferreira, C. M.; Gordiets, B. F.; Osipov, A. I. *Plasma Kinetics in Atmospheric Gases*; Springer: Berlin, 2000
(66) Vankan, P.; Schram, D. C.; Engeln, R. *Chem. Phys. Lett.* **2004**, *400*, 196.
(67) Jackson, B.; Pearson, M. *J. Chem. Phys.* **1992**, *96*, 2378.
(68) Rettner, C. T. *Phys. Rev. Lett.* **1992**, *69*, 383.
(69) Mannella, G. G. *Chem. Rev.* **1963**, *63*, 1.
(70) Sarrette, J.-P.; Rouffet, B.; Ricard, A. *Plasma Processes Polym.* **2006**, *3*, 120.
(71) Geppert, W. D.; Thomas, R.; Semaniak, J.; Ehlerding, A.; Millar, T. J.; Österdahl, F.; Ugglas, M. A.; Djuric, N.; Paál, A.; Larsson, M. *Astrophys. J.* **2004**, *609*, 459.